

Effect of ultra-fast heat treatment on the subsequent formation of mixed martensitic/bainitic microstructure with carbides in a crmo medium carbon steel

Papaefthymiou, Spyros; Banis, Alexandros; Bouzouni, Marianthi; Petrov, Roumen H.

DOI

[10.3390/met9030312](https://doi.org/10.3390/met9030312)

Publication date

2019

Document Version

Final published version

Published in

Metals

Citation (APA)

Papaefthymiou, S., Banis, A., Bouzouni, M., & Petrov, R. H. (2019). Effect of ultra-fast heat treatment on the subsequent formation of mixed martensitic/bainitic microstructure with carbides in a crmo medium carbon steel. *Metals*, 9(3), Article 312. <https://doi.org/10.3390/met9030312>

Important note

To cite this publication, please use the final published version (if applicable). Please check the document version above.

Copyright



Other than for strictly personal use, it is not permitted to download, forward or distribute the text or part of it, without the consent of the author(s) and/or copyright holder(s), unless the work is under an open content license such as Creative Commons.

Takedown policy

Please contact us and provide details if you believe this document breaches copyrights. We will remove access to the work immediately and investigate your claim.

Article

Effect of Ultra-Fast Heat Treatment on the Subsequent Formation of Mixed Martensitic/Bainitic Microstructure with Carbides in a CrMo Medium Carbon Steel

Spyros Papaefthymiou ^{1,*} , Alexandros Banis ¹, Marianthi Bouzouni ^{1,2} and Roumen H. Petrov ^{3,4} 

¹ Laboratory of Physical Metallurgy, Division of Metallurgy and Materials, School of Mining & Metallurgical Engineering, National Technical University of Athens, 9, Her. Polytechniou str., Zografos, 15780 Athens, Greece; alexbanis@central.ntua.gr (A.B.); mbouzouni@elkeme.vionet.gr (M.B.)

² Department of Physical Metallurgy and Forming, Hellenic Research Centre for Metals S.A.—ELKEME S.A., 61st km Athens-Lamia Nat. Road, 32011 Oinofyta, Viotia, Greece

³ Department of Electrical Energy, Metals, Mechanical constructions & Systems, Ghent University, Technologiepark 46, 9052 Ghent, Belgium; roumen.petrov@ugent.be

⁴ Department of Materials Science and Engineering, Delft University of Technology, Mekelweg 2, 2628CD Delft, The Netherlands

* Correspondence: spapaef@metal.ntua.gr; Tel.: +30-210-772-4710

Received: 5 February 2019; Accepted: 4 March 2019; Published: 10 March 2019



Abstract: The current work focuses on complex multiphase microstructures gained in CrMo medium carbon steel after ultra-fast heat treatment, consisting of heating with heating rate of 300 °C/s, 2 s soaking at peak temperature and subsequent quenching. In order to better understand the microstructure evolution and the phenomena that take place during rapid heating, an ultra-fast heated sample was analyzed and compared with a conventionally treated sample with a heating rate of 10 °C/s and 360 s soaking. The initial microstructure of both samples consisted of ferrite and spheroidized cementite. The conventional heat treatment results in a fully martensitic microstructure as expected. On the other hand, the ultra-fast heated sample shows significant heterogeneity in the final microstructure. This is a result of insufficient time for cementite dissolution, carbon diffusion and chemical composition homogenization at the austenitization temperature. Its final microstructure consists of undissolved spheroidized cementite, nano-carbides and martensite laths in a ferritic matrix. Based on EBSD and TEM analysis, traces of bainitic ferrite are indicated. The grains and laths sizes observed offer proof that a diffusionless, massive transformation takes place for the austenite formation and growth instead of a diffusion-controlled transformation that occurs on a conventional heat treatment.

Keywords: ultra-fast heating; martensite/bainite; diffusionless transformations; AHSS

1. Introduction

Over the last years the research focus was on both strength and toughness increase of advanced high strength steels (AHSS). This was achieved either by introducing multiphase microstructures embedding bainitic ferrite, retained austenite and/or martensite in a ferritic matrix (dual phase—DP, TRansformation Induced Plasticity—TRIP, complex phase—CP steels to name a few), or by getting use of the twinning effect of austenite (Twinning Induced Plasticity—TWIP steels), or by using alloying elements (Mn and AlMn steels) or currently by developing steels with submicron (nano-scaled) mixed grain structure including tempered martensite, retained austenite and bainite (e.g., quenching

& partitioning—Q&P steels) [1–3]. In all these developments attention was given to the chemical composition and the tailored made heat treatment cycles, many of which are achieved in two or more stages. Till now, the effect of increased heating rate during the final heat treatment was not incorporated in the steel development strategies. Fast and ultra-fast heating rates are usually obtained by induction heating combined with a subsequent water or oil quenching. Although there is no clear specification what the borders between normal, fast and ultra-fast heating rates in the existing literature are, the following can be considered: Low and normal heating rates are between 1 °C/s and 20 °C/s, high heating rates are between 20 °C/s and 100 °C/s and ultra-fast heating rates are these above 100 °C/s. As induction heating is currently introduced as part of the forming process chain (press hardened and air hardened steels) replacing classical gas furnaces, the effect of rapid heating in the ferrite-to-austenite transformations and the carbide dissolution must gain more attention [4–7]. At increasing heating rates above 100 °C/s the resulting microstructures differ from those after conventional heat treatments [4,5,8,9]. The reason is that the ferrite to austenite phase transformation during ultra-fast heating creates chemically and structurally (morphologically) heterogeneous austenite with very fine grains which transforms after quenching to mixtures of bainite & martensite and finely dispersed carbides [10]. The latter in combination with the dislocation density introduced during displacive transformations will further impede the final thickness of martensitic or bainitic plates and sheaves respectively [11–13]. Moreover, the presence of substitutional atoms e.g., Cr and Mn, which tend to segregate at interfaces can modify the local equilibrium and affect the subsequent phase transformations [14–18]. Other alloying elements such as Si suppress the carbide precipitation during the bainitic transformation and stimulate the retention of austenite at room temperature. The above mechanisms may lead to formation of multiphase microstructures consisting of martensitic, bainitic ferritic plates with high and low carbon content often accompanied with M–A (martensite–austenite) islands [19].

With the recent developments in microstructure and crystallographic analysis (scanning and transmission electron microscopy SEM & TEM—STEM, electron backscatter diffraction EBSD, transmission Kikuchi diffraction—TKD) it is possible to distinguish and quantify these nano—constituents in order to understand the mechanism of their formation and their impact on the mechanical properties [20].

The ultra-fast heat treatment e.g., via induction heating utilizes the effect of the rapid heating to restrict the austenite grain size and its chemical composition prior to quenching. In this way, a mixed martensite/bainite microstructure matrix with embedded carbides can be obtained in one step paving the way for increased and more isotropic mechanical properties of the treated steel. The ultra-fast heat treatment was introduced in sheets and tubes by Cola et al. [21–24] in which a large variety of refined microstructures and properties were derived. The ultra-fast heat treatment in steels affects the microstructure additionally by creating a conditions ferrite -to-austenite phase transformation to start and progress in non-recrystallized or partially recrystallized (recovered) matrix which reflects in better mechanical properties, namely increase of both strength and elongation [25–27]. The impact of heating rate on phase composition and volume fraction of individual micro-constituents has been studied as well [28]. Ultra-fast heating of a low-carbon steel to inter-critical peak temperature prompts to a complex microstructure of the ferritic matrix, which comprises of recrystallized and recovered grains [29–31]. Thus, the local mechanical behavior of the ferritic matrix may drastically vary upon the local dislocation density.

Cerda et al. [32,33] studied the effect of ultra-fast heating on the recrystallization of ferrite. In another study the same authors [34–36] explained the impact of the initial microstructure on the austenite formation mechanism and that the nucleation step can be obtained either by diffusion or diffusionless mechanisms, while the growth stage can be controlled by either diffusion or the interfaces of the constituents in what is called ‘massive transformation’. Concerning the diffusionless mechanisms, Kaluba et al. [37–39] supported a supposed bainitic transformation mechanism to form austenite when high heating rates are applied. Papaefthymiou et al. [40,41] studied the impact of rapid

heating on the dissolution kinetics of cementite, on the formation of austenite and explained the reasons for bainite presence in the final microstructures. Coupling experiment and simulation techniques Bouzouni et al. [42,43] studied the carbide dissolution and modeled the phase transformations during ultra-fast heating while Banis et al. [44] studied the presence of bainite in the microstructure using scanning and transmission electron microscopy techniques.

Scope of this paper is to identify, characterize and compare qualitatively, but also quantitatively where possible, the microstructures of a chromium molybdenum (CrMo) medium carbon steel formed after conventional heating, isothermal soaking and quenching and the one after heating with 300 °C/s and soaked for maximum of 2 s at the austenitization peak temperature. For a deeper understanding of the effect of the ultra-fast reheating on the microstructure, the rapid reheating is simulated. With the help of DICTRA we could identify the effect of short-range diffusion in the proximity of carbides. The element segregation in grain boundaries is closely followed and its role in the microstructure evolution is studied. For this reason, ThermoCalc and Dictra modelling results are presented and discussed.

2. Materials and Methods

In order to examine the microstructure evolution under ultra-fast heat treatment a hot-rolled, medium carbon, chromium-molybdenum (CrMo) steel (42CrMo4) was used. The chemical composition can be seen in Table 1.

Table 1. The chemical composition in wt. % for the steel that was used for both samples.

| C | Si | Mn | S | P | Cr | Mo | Ti | N | Fe |
|------|-----|------|--------|-------|------|-----|-------|------|------|
| 0.43 | 0.4 | 1.43 | 0.0135 | 0.013 | 1.23 | 0.1 | <0.05 | 0.01 | rest |

Controlled-heating experiments were performed in a Bähr 805A quench dilatometer (TA Instruments, New Castle, DE, USA). Samples for dilatometry test with length 10 mm, width 2 mm and thickness of 1 mm were cut from the cross sections of hot rolled bars. The temperature was controlled by an S-type thermocouple, spot welded to the midsection of each test sample.

The heat treatments for the conventional (CH) and the ultra-fast (UFH) heat treated samples were performed using induction heating and are summarized in Figure 1a. The T_{peak} is significantly increased in the ultra-fast heat-treated sample in order to avoid the inter-critical region because the increased heating rate shifts the A_{c3} temperature to higher values [27,45]. The initial microstructure of both samples consisted of ferrite and spheroidized cementite as shown in Figure 1b. The spheroidized cementite can be better seen in the TEM micrograph of Figure 1c.

For microstructure characterization electron microscopy techniques were combined. SEM and TEM were utilized to observe the micro-constituents and STEM/EDS for their chemical analysis while EBSD was utilized to further study the microstructural constituents, their size, crystallographic orientation and the prior (parent) austenite [46] orientation and morphology. ThermoCalc® and DICTRA [45] were employed to study the diffusion of alloying elements and the carbide dissolution during ultra-fast heating and isothermal holding at peak temperature. The samples for the microstructure characterization were cut from the center of the dilatometric specimens and were then prepared, in accordance with the standard procedure, by grinding and polishing to a mirror-like finish using 6 µm and 1 µm diamond pastes and etching in a solution of 2% v/v HNO₃ in ethanol (Nital 2%) for 5 s at 20 °C to reveal the microstructure. For TEM analysis, disk samples were cut from the dilatometry specimens, then they were manually ground to a thickness of 20 µm and then brought to their final thickness using the Precision Ion Polishing System (PIPS).

For Scanning Electron Microscopy (SEM) analysis a JEOL6380LV SEM operating at 20 kV in SE (BSE) mode was used. For Electron Back-Scatter Diffraction (EBSD) analysis, a FEI Quanta TM 450-FEG-SEM was operated under the following settings: The accelerating voltage was 20 kV with a beam current corresponding to a FEI spot size of 5, aperture size of 30 µm and working distance of 11 mm. The sample was tilted by 70° toward the EBSD detector, and the resulting patterns

were acquired on a hexagonal scan grid by a Hikari detector operated with EDAX TSL—OIM-Data Collection version 6 software (AMETEK Materials Analysis Division, Mahwah, NJ, USA). The EBSD scans were performed at a step size of 0.5 μm and 0.05 μm . The corresponding orientation data were post-processed with EDAX-TSL-OIM-Data Analysis version 7 software (AMETEK Materials Analysis Division, Mahwah, NJ, USA) using the following grain definition: Misorientation with neighboring grains higher than 5°, minimum number of points per grain was 2 and confident index (CI) higher than 0.1. Based on the EBSD data a prior austenite grains were reconstructed by means of the ARPGE software developed by C. Cayron [46]. A Jeol 2100 HR, 200kV Transmission Electron Microscope (TEM) was used for the TEM analysis in bright field imaging mode. Thermodynamic and kinetic calculations have been conducted using the TCFE8 database from ThermoCalc® software (Version 2018a, ThermoCalc Software AB, Solna, Sweden) in conjunction with the MOBFE3 database from DICTRA software (Version 2018a, ThermoCalc Software AB, Solna, Sweden). For the calculation of the CCT diagrams, the models of Kirkaldy [47,48] and Bhadeshia [49,50] were used taking into account the chemical composition of the steel and the grain size of the parent austenite. During the calculations, homogeneity of the composition and the grain sizes is assumed, while the conditions assume equilibrium.

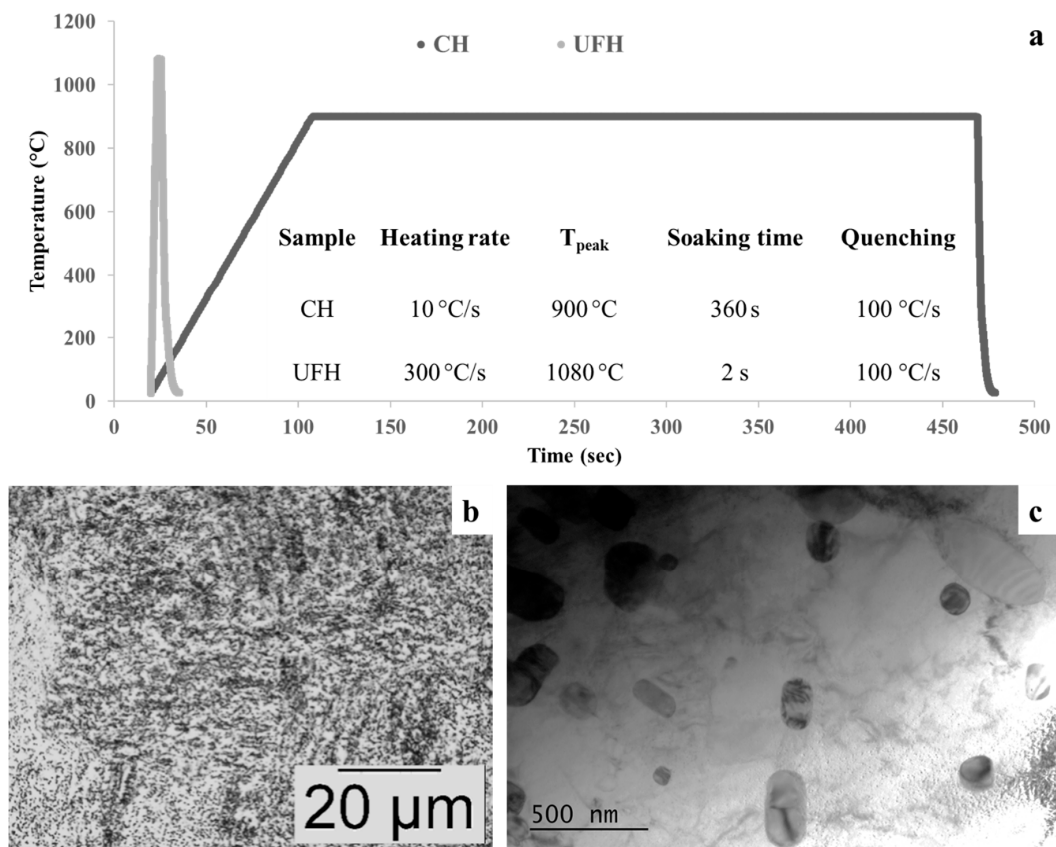


Figure 1. (a) The parameters of the two heat treatments that were studied, (b) the initial microstructure of both samples, as seen in the OM, consisted of ferrite (white) and spheroidized cementite (dark grey) (c) a bright field TEM image of the spheroidized cementite in the initial microstructure.

3. Results and Discussion

3.1. Material Modelling

Figure 2a depicts the phase diagram of the CrMo steel calculated with ThermoCalc® in order to predict the stable phases expected in equilibrium. Using DICTRA, the dissolution of carbides (cementite and M_7C_3), the ferrite-to-austenite transformation and the chemical gradients across interfaces between

carbides and the matrix (α/γ) were studied during ultra-fast heating and holding at 1080 °C, a temperature well within the austenite range. $M_{23}C_6$ carbide was not considered to affect the α to γ transformation hence the results of $M_{23}C_6$ dissolution were excluded for simplicity. The chemical composition of the phases was determined with Thermocalc[®] at equilibrium by taking the volume fractions of the components into consideration. Silicon (Si), due to its minor solubility in carbides is removed from the system, which takes into account the elements Fe, C, Cr, Mn and Mo. The carbides were assumed with spherical shape and initial size was set to 5 nm as derived by TEM observations. According to Papaefthymiou [40] and De Knif et al. [27], with increasing heating rates normal to the ultra-fast, a shift in the A_{c1} and A_{c3} temperatures to higher values was observed. Specifically, as shown in Figure 2b, for 300 °C/s heating rate, the austenite transformation starts at 810 °C (A_{c1}) and ends at 900 °C (A_{c3}) which are higher than the temperatures calculated on equilibrium phase diagram. Also, the martensite transformation during quenching starts at 290 °C (M_s). At the interfaces of carbides with ferrite or austenite, thermodynamic equilibrium (local equilibrium hypothesis) was assumed.

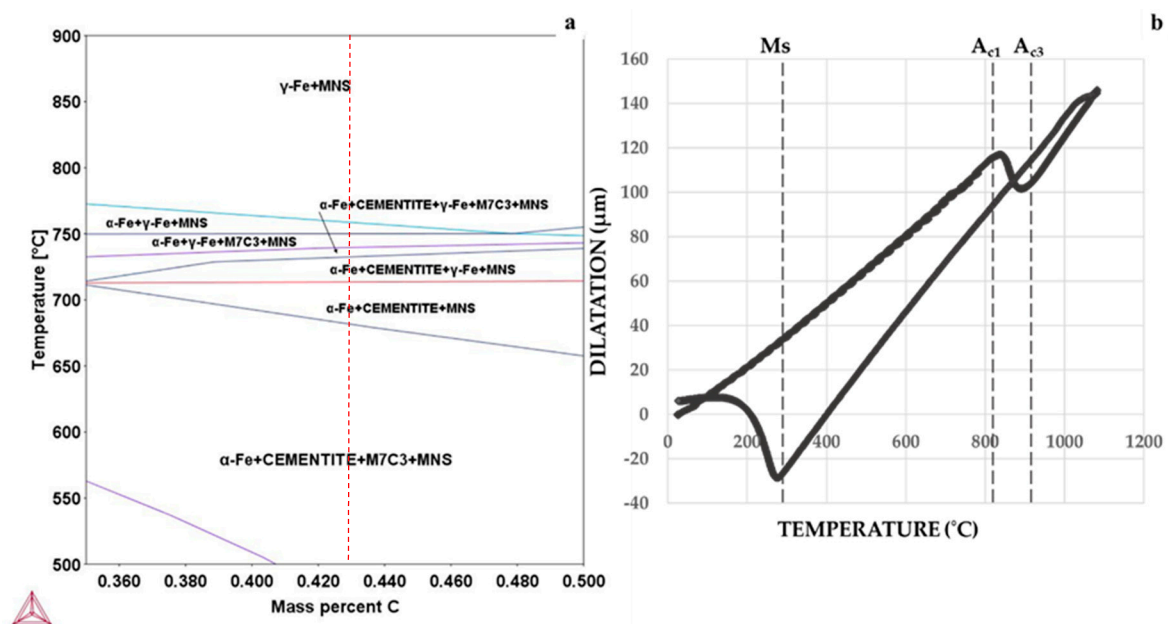


Figure 2. (a) Isopleth of the phase diagram of CrMo steel calculated using Thermocalc[®]. The dashed line indicates the C content, (b) Temperature-Dilatation graph for the UFH sample measured with a heating rate of 300 °C/s and cooling rate of 100 °C/s. The transformation temperatures (A_{c1} , A_{c3} , M_s) derived from this diagram.

3.2. Microstructure Comparison

The microstructure of the conventional sample is shown in Figure 3a. The volume fraction of martensite appears to be 100% while there is no evidence for presence of cementite or undissolved carbides. The size of martensite laths is very similar and shows no deviations, while it is larger than the average lath size of the UFH sample as shown in Figure 3b. According to this figure, the microstructure of the UF samples demonstrates advanced complexity with significant heterogeneity concerning the grain sizes and the microstructural constituents. Coarse martensite laths are apparent in both CH and UFH while fine bainitic laths next to spherical particles possibly partial dissolved carbides or retained austenite were observed in UFH (Figure 3b).

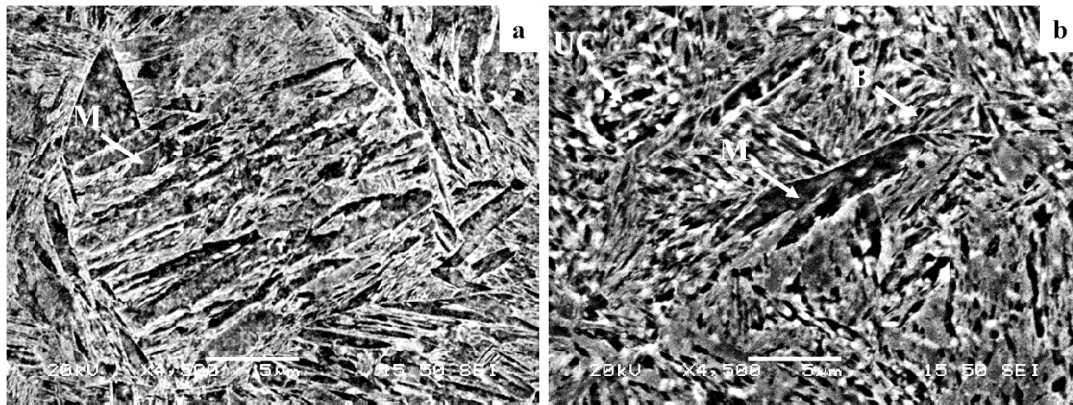


Figure 3. SEM images of the CH (a) and the UFH sample (b). The CH consists of a martensitic (M) matrix while the UFH sample consists of a martensitic (M) matrix with undissolved cementite (UC) and bainite (B).

3.3. Grain Size Analysis

From the EBSD analysis of the grain size, the coarser plate in CH was measured at an average $3.77\ \mu\text{m}$ while finer plates were measured at an average $1.93\ \mu\text{m}$ in UFH indicating that the martensitic laths in UFH are significantly refined compared to CH. Fine austenite size is a reason for decrease of the M_s temperature as reported by Lee et al. [51]. The ARPGE 2.4 software developed by C. Cayron [46] in EPFL-LMTM, was used in automatic mode to reconstruct the prior austenite grains and the normal direction inverse pole figure (ND IPF) maps of the reconstructed prior austenite grains (PAGs) for both samples are shown in Figure 4a,b. For the UFH (Figure 4b), these PAGs have significantly smaller size than the CHTS while the deviation between the PAGs in the UFH is quite large. In particular, the average calculated grain diameter (referred in this paper as grain size) for the PAGs is $11.12\ \mu\text{m}$ for the CH and $7\ \mu\text{m}$ for the UFH. As seen in Figure 4c, for the conventional heat-treatment, almost 40% of the PAGs have a diameter of $20\ \mu\text{m}$. After quenching, the martensitic laths in the final microstructure vary in size between 1.6 and $3.6\ \mu\text{m}$ (Figure 4d). On the other hand, concerning the UF heating, the PAG size has greater variation. Specifically, most of the PAGs have a diameter between 8 and $14\ \mu\text{m}$ (Figure 4c). The reason for these smaller austenite grains is most likely that austenite nucleates at the interfaces of undissolved carbides (cementite and M_7C_3) with ferrite and at ferrite/ferrite interfaces [15,34,35]. Moreover, undissolved carbides have a pinning effect, thus, impeding further the growth of austenite grains. After quenching, the microstructural constituents mostly have sizes between 0.2 and $1.8\ \mu\text{m}$ resulting in a very fine microstructure. The type of Undissolved Carbides (UCs) was identified with index patterns from bright field TEM images of the UFH sample as seen in Figure 5a,b.

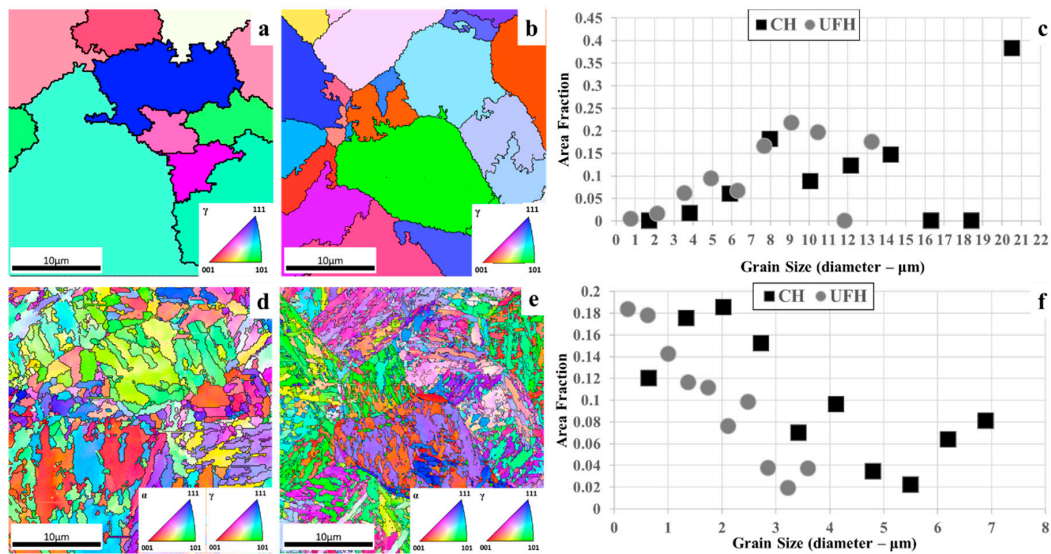


Figure 4. (a) IPF map of the reconstructed PAGs of the CH sample with the use of the ARPGE [46] software, (b) IPF map of the reconstructed PAGs of the UFH sample with the use of the ARPGE [46] software, (c) grain size chart for the PAGs of both samples indicating the refinement of austenite in UFH, (d) IPF map of the final microstructure of the CH sample, (e) IPF map of the final microstructure of the UFH sample, (f) grain size chart for the final microstructure of both samples indicating the refinement of grains and laths in the UFH.

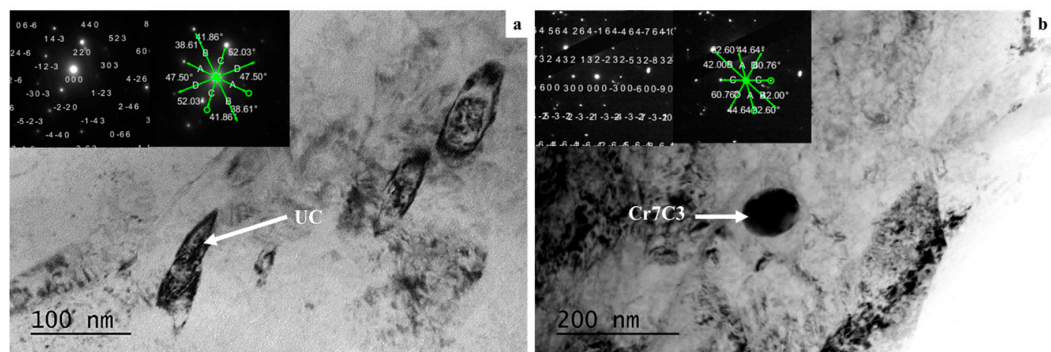


Figure 5. (a) Undissolved Cementites (UCs) are present in the final microstructure of the UFH sample. The undissolved cementite indexed pattern is shown on the top left corner (b) Undissolved Cr₇C₃ are present on grain boundaries in the final microstructure of the UFH sample some of these UCs are also found.

According to the sizes of the PAGs calculated from EBSD, the CCT diagrams were plotted using the models of Kirkaldy [47,48] and Bhadeshia [49,50]. From these diagrams, the transformation starting temperatures for bainite (B_s) can be seen in Figure 6a. During the calculation, the chemical composition was assumed homogeneous and the grain size varied between 1 μm and 7 μm. Also, the calculations are made assuming equilibrium conditions. From this diagram it can be concluded that as the grain size of the parent austenite is decreasing, the curve showing the position of the B_s shifts to the left (i.e., decreasing the incubation time), thus making it possible to obtain bainite during quenching with 100 °C/s. According to this, some PAGs with diameter smaller than ~7 μm and with 0.43 wt.% carbon content that are found in the microstructure, are able to transform into bainite. For austenite grain size larger than 7 μm the B_s temperature is shifted to the right hand side of the diagram of Figure 6a, which explains why bainite cannot form with this cooling rate and only martensite forms rapidly at temperatures below the M_s temperature (292 °C). Nevertheless, during UFH, large heterogeneity is expected in the distribution of carbon in the PAGs based on references [40,41]. Therefore, another CCT

diagram was plotted in Figure 6b. In this diagram, the transformation temperatures for bainite were calculated for a variation of carbon contents while the PAG size was assumed stable at 7 μm . This size was selected, because it represented the average grain size that was calculated for the PAGs as mentioned before in Figure 4c. Again, in this calculation, equilibrium conditions were assumed as well as homogeneity in the austenitic grain size. Though, as seen in Figure 6, for decreasing carbon content in the steel and for the given PAG size, the bainitic transformation starts at shorter time in comparison to the model where high carbon content was considered (B_s shifts to the left), while the M_s shifts to higher temperatures. Specifically, the M_s temperatures for 0.1%, 0.2%, 0.3% and 0.4% carbon content are calculated at 417°, 379°, 340° and 304 °C respectively. Therefore, according to the calculated CCT diagrams it is also possible to obtain bainite at the given conditions.

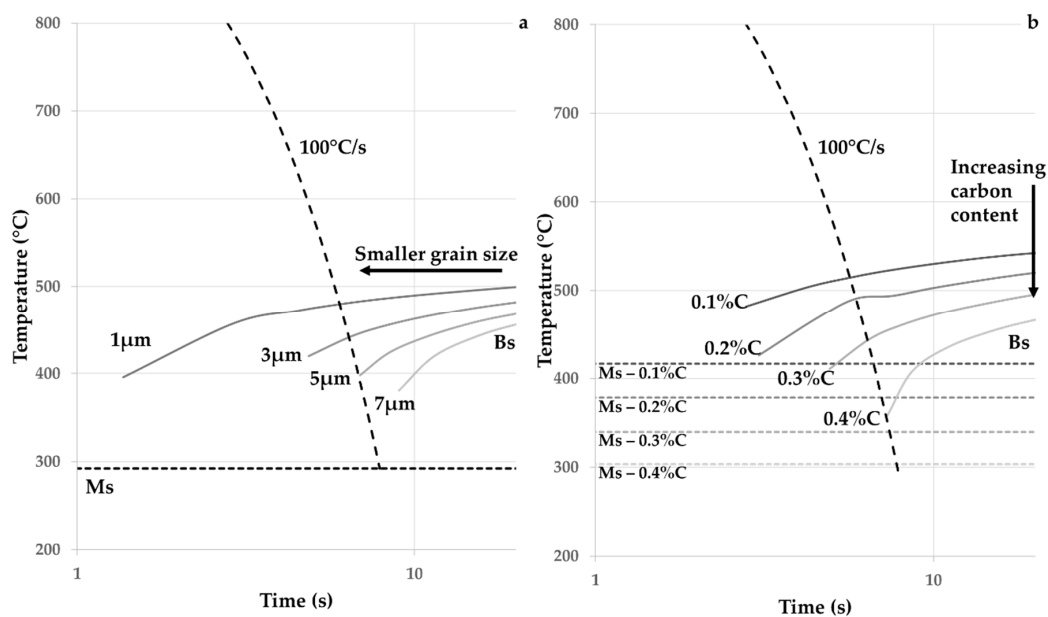


Figure 6. (a) the B_s temperatures as they were calculated in the CCT diagrams [47–50] for varying PAG sizes for a certain chemical composition (b) the B_s temperatures as they were calculated in the CCT diagrams [47–50] for varying carbon concentrations for a certain PAG size. The M_s temperatures are also shifting for increasing carbon content from 417 °C to 304 °C.

3.4. Microstructural Constituents Analysis

Further investigation of UFH based on grain average Image Quality (GAIQ) [51] confirmed the presence of ferrite, while there are strong indications for bainitic laths or martensite laths with low C content. This technique depends on the distortion of the lattice of each constituent and the diffraction pattern it produces. Depending on the quality of the diffraction pattern, the image quality will differentiate for each constituent during the analysis of the EBSD data. This technique has been used thoroughly to distinguish ferrite from martensite and bainite [52–55], but in this case, the selected cut off ranges have to be defined very carefully having in mind that the dislocation density and corresponding lattice distortions in bainite and martensite are very close. Green areas denote grains with low grain average image quality with possibly high dislocation density regions that most probably correspond to martensitic grains, blue areas denote the grains with the highest GAIQ and possibly with the lowest dislocation density and correspond to ferritic areas, whereas the red areas can be bainitic laths or martensitic laths with low C% (Figure 7a). According to Pinard et al. [53], higher lattice distortion in martensite leads to a lower quality of its diffraction patterns. According to the GAIQ, the percentage of martensite (green) is 54.2%, that of ferrite is 1.3% and the percentage of low carbon martensite or bainite is 40.3%. To make a closer approximation of the percentage of the aforementioned structure constituents (martensite, bainite, ferrite), another GAIQ map (Figure 7b) was used including

the misorientation angles. According to Papaefthymiou et al. [40], misorientation angles between 17–47° (indicated in black) correspond to PAGBs, angles between 48–55° (red) correspond to bainite while those between 57–65° (blue) correspond to martensite. From this map and from the chart provided, it appears that only a small fraction of misorientation angles corresponds to bainite. This chart depicts the misorientation angle (red line) correlated to a random distribution of misorientation (MacKenzie type) while the rectangles indicate the delineated areas of PAGs, bainite and martensite on the GAIQ map. When combining these two maps, it can be said that only a small part of the red colored laths corresponds to bainite while the rest corresponds to low-carbon martensite. In order though to better distinguish bainite from martensite, further research must be carried out. More specifically this refers to the investigation of the carbon content distribution using methods such as EPMA and TEM-EDS analysis. Bainitic morphologies were already clearly observed on TEM as shown in Figure 7c and in SEM (Figure 7d). They consist of small aligned precipitates intercepting the laths and, even more nano-precipitates are stacked on the lath boundaries. Laths with increased dislocation density that appear darker in the micrographs are characterized as martensitic laths, whereas laths that appear brighter are characterized as bainitic [31]. The precipitated carbides (PCs) seen in Figure 7c are probably cementite however due to their small size, they were not able to be indexed correctly. The presence of bainite in the microstructure of ultra-fast heat-treated steels is supported also in the most recent work of Cerda et al. [56] on a 0.2% and a 0.44% carbon steels, where they observed bainitic morphologies in OM and SEM.

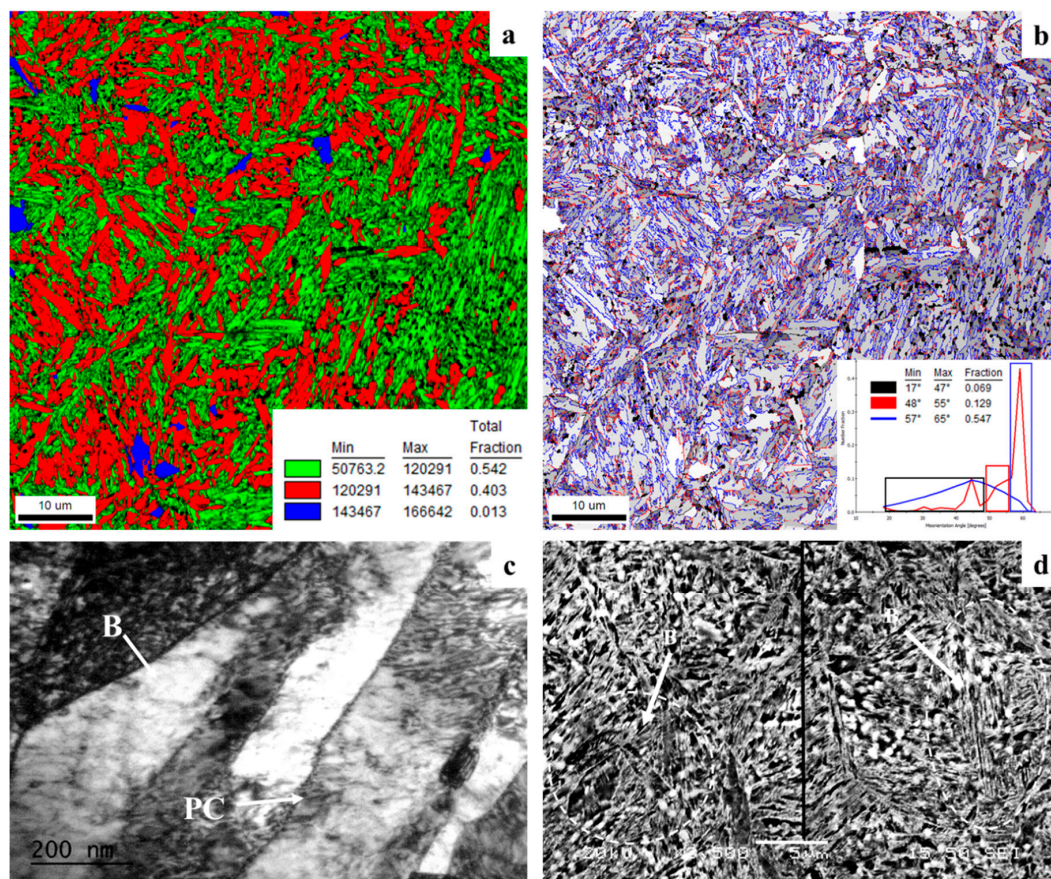


Figure 7. (a) Color coded GAIQ map for the UFH sample. Martensite is indicated in green, ferrite in blue while low-carbon martensite and bainite in red, (b) gray-scale GAIQ map of the same area with misorientation angles indicating the boundaries between PAGs (black), bainite (red) and martensite (blue), (c) The presence of bainite has been observed in TEM and (d) in SEM. The two SEM micrographs indicate the presence of bainitic areas in the microstructure.

Austenite was also found in the microstructure of both samples. Figure 8a,b shows the phase maps for CH and UFH samples which proves the existence of retained austenite. In the case of the CH sample only a very small amount (0.2%) of austenite was detected, while in the UFH sample the identified amount of austenite is 4.2%. In order to obtain the austenite amount, other constituents with FCC structure (such as MnS) had to be excluded and, thus, the K-S relationship for α - γ : $\langle 112 \rangle 90^\circ$ was used.

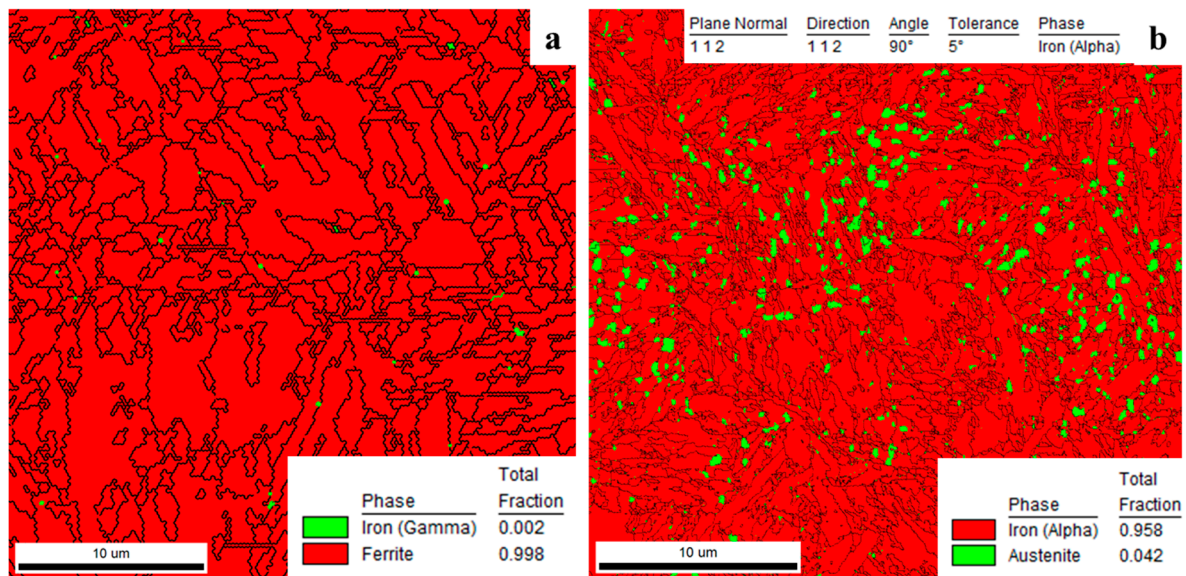


Figure 8. (a) Phase map of the CH sample which consists of 0.2% austenite, (b) phase map of the UFH sample in which the amount of austenite is considerably higher (4.2%).

3.5. Effect of Chemical Heterogeneity at T_{peak}

The results from DICTRA for the UFH sample indicate that cementite (θ) and M_7C_3 remain undissolved. Figure 9a–d show the chemical heterogeneity in austenite at T_{peak} as a result of the rapid heating. The substitutional elements Cr, Mn, Mo accumulate in the vicinity of the carbide interface with austenite that variation of Cr, Mn, Mo at the θ/γ (cementite/austenite) and M_7C_3/γ interface at T_{peak} temperature. Particularly, Cr affects the interface movement the most as it presents a strong affinity with C and tends to co-segregate with it at carbide/ γ interfaces leading to an impediment in its diffusion, reaching up to 18 wt. % in the vicinity of θ/γ interface, while the Cr content close to the M_7C_3/γ interface increases up to 60 wt. %. Therefore, the interface movement is mainly controlled by the diffusion of substitutional alloying element (Cr, Mn, Mo). As carbides dissolve, Cr, Mn and Mo are transferred from carbides to austenite. The substitutional atoms are also transferred from γ to carbides in order to maintain local equilibrium. Hence, the enrichment in substitutional atoms in the outer layer of γ stabilizes the carbides. The slower movement of the M_7C_3/γ interface, compared to the advance of θ/γ interface, shows that less carbon is in solution in austenite formed nearby M_7C_3 (0.4 wt. % C) than austenite next to θ (~1 wt. % C) at T_{peak} . In order to maintain the local equilibrium at the interface, Mn, Cr and Mo have to be redistributed between carbides and austenite. In the case of conventional heating, the carbides dissolve completely during the thermal cycle and the chemical gradients are expected to be homogenized since there is sufficient time for diffusion of atoms. Figure 9e indicates that carbide dissolution at 900 °C at the conventional thermal cycle is accomplished beyond 40 s.

The chemical heterogeneity in austenite indicates that regionally different CCT diagrams are applied in each area upon cooling and thus the coexistence of bainite/martensite found in microstructural analysis (Figures 3b and 7c,d) can be explained. Moreover, areas enriched in C reaching up to 1% wt lead to small fractions of retained austenite after quenching which is validated by the phase map (Figure 8b).

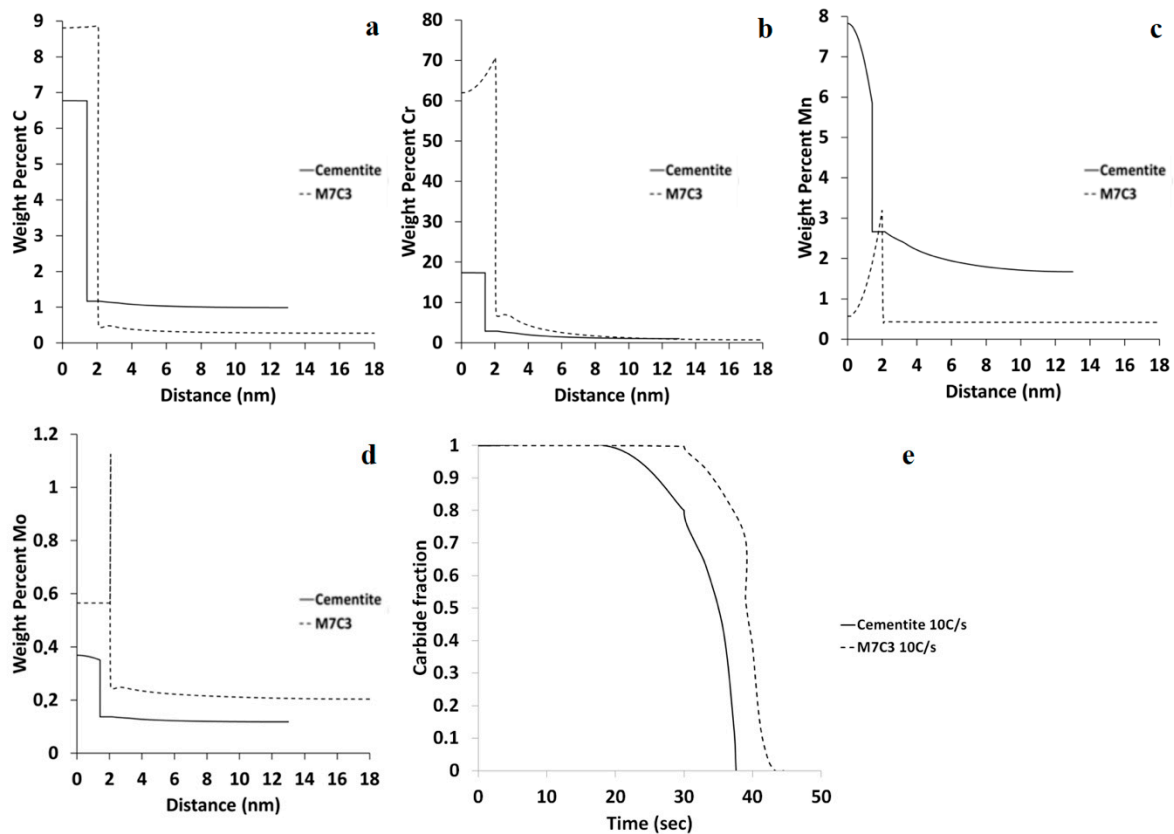


Figure 9. Composition profiles during carbide dissolution in austenite at T_{peak} for the UFH sample, spherical cell, size 5 nm (a) C, (b) Cr, (c) Mn, (d) Mo content, respectively. (e) Diagram of carbide fraction change in conjunction with time during dissolution for heating rate 10 °C/s.

4. Conclusions

This study provides a detailed analysis of mixed microstructures obtained after the application of an ultra-fast heat treatment (UFH) in comparison to the microstructures obtained after a conventional heat treatment (CH). The data prove that the increased heating rate results in finer austenite grains at the peak austenite temperature (T_{peak}) compared to conventional heating. The difference in austenite size affects the phase transformations during quenching. In UFH and CH heat-treated samples, submicron and nanostructured ferrite and martensitic laths were apparent as revealed via EBSD based on the difference of the IQ diffraction patterns. However, in UFH, the presence of bainite (or bainitic ferrite) was distinguished due to the carbide precipitation, observed at the interface of bainitic ferrite laths since the IQ values are similar to martensite. In the UFH sample, undissolved spherical carbides were also observed. The simulation results showed that at high heating rates the time for diffusion is limited. The substitutional atoms accumulate near the interface of carbides with austenite. This impedes the dissolution of carbides and leads to chemical heterogeneity in the microstructure. Austenite with both low and high carbon content leads to different transformation products after quenching to room temperature. Thus, both martensite and bainite are present in the final microstructure after the UFH. In this way the UFH microstructure consists of martensite/bainite submicron laths, undissolved carbides (cementite and M_7C_3), refined ferrite and small fraction of retained austenite, whereas the CH microstructure contains martensite and a very small fraction of austenite after the quench.

Further research is essential on ultra-fast heat-treated steels in order to fully control the microstructure evolution, the phases on the final microstructure and to tailor their mechanical properties.

Author Contributions: Conceptualization, S.P.; methodology, S.P., A.B., M.B.; software, M.B.; validation, M.B., A.B., S.P.; formal analysis, S.P.; investigation, S.P., A.B., M.B.; resources, S.P., R.H.P.; data curation, A.B., M.B.; writing—original draft preparation, S.P., A.B., M.B.; writing—review and editing, S.P., R.H.P.; visualization, M.B., A.B.; supervision, S.P.; project administration, S.P.

Funding: This research received no external funding.

Acknowledgments: The authors express their gratitude to the Hellenic Research Centre for Metals–ELKEME S.A. and Thermocalc for support to this research. We thank Petros Tsakiridis from the National Technical University of Athens for his support with Transmission Electron Microscopy. We also thank Athanasios Vazdirvanidis from ELKEME S.A. for his support with EBSD measurements.

Conflicts of Interest: The authors declare no conflict of interest.

References

- Bleck, W.; Frehn, A.; Papaefthymiou, S. Microstructure and Tensile Properties in Dual Phase and Trip Steels. *Steel Res. Int.* **2004**, *75*, 704–710. [CrossRef]
- Ponge, D.; Zhang, H.; Raabe, D. Designing quadplex (four-phase) microstructures in an ultrahigh carbon steel. *Mater. Sci. Eng. A* **2014**, *612*, 46–53.
- Adamczyk, J.; Opiela, M. Influence of the thermo-mechanical treatment parameters on the inhomogeneity of the austenite structure and mechanical properties of the Cr-Mo steel with Nb, Ti, and B microadditions. *J. Mater. Process. Technol.* **2004**, *157–158*, 456–461. [CrossRef]
- Vieweg, A.; Ressel, G.; Prevedel, P.; Raninger, P.; Panzenböck, M.; Marsoner, S.; Ebner, R. Induction hardening: Differences to a conventional heat treatment process and optimization of its parameters. *IOP Conf. Mater. Sci. Eng.* **2015**, *119*, 012019. [CrossRef]
- Vieweg, A.; Ressel, G.; Prevedel, P.; Marsoner, S.; Ebner, R. Different Cooling Rates and Their Effect on Morphology and Transformation Kinetics of Martensite. In Proceedings of the International Conference on Martensitic Transformations: Chicago, Chicago, IL, USA, 9–14 July 2017.
- Orlich, J. *Atlas zur Wärmebehandlung der Stähle, Max-Planck-Institut für Eisenforschung*; Verlag Stahleisen mbH: Düsseldorf, Germany, 1973. Available online: <https://onlinelibrary.wiley.com/doi/abs/10.1002/maco.19730241030> (accessed on 8 March 2019).
- Rudnev, V. Subject-oriented assessment of numerical simulation techniques for induction heating applications. *Int. J. Mater. Prod. Technol. (IJMPT)* **2007**, *29*, 43–51. [CrossRef]
- Rudnev, V. *Induction Hardening Cast Iron, Heat Treating Progress*; ASM Int.: Materials Park, OH, USA, 2003; pp. 27–32.
- Zinn, S.; Semiatin, S. *Elements of Induction Heating: Design, Control and Applications*; ASM International: Materials Park, OH, USA, 1988; ISBN 978-0-87170-308-8.
- Lan, L.; Chang, Z.; Fan, P. Exploring the Difference in Bainite Transformation with Varying the Prior Austenite Grain Size in Low Carbon Steel. *Metals* **2018**, *8*, 988. [CrossRef]
- Garcia-Mateo, C.; Jimenez, J.A.; Lopez-Ezquerro, B.; Rementeria, R.; Morales-Rivas, L.; Kuntz, M.; Caballero, F.G. Analyzing the scale of the bainitic ferrite plates by XRD, SEM and TEM. *Mater. Charact.* **2016**, *122*, 83–89. [CrossRef]
- Cornide, J.; Garcia-Mateo, C.; Capdevila, C.; Caballero, F.G. An assessment of the contributing factors to the nanoscale structural refinement of advanced bainitic steels. *J. Alloys Compd.* **2013**, *577*, S43–S47. [CrossRef]
- Caballero, F.G. Martensite and bainite in nanocrystalline steels: understanding, design and applications. In Proceedings of the ESOMAT 2015—10th European Symposium on Martensitic Transformations, Antwerp, Belgium, 14–18 September 2015.
- Speich, G.; Szirmai, A.; Richards, M. Formation of austenite from ferrite and ferrite-carbide aggregates. *Trans. TMS-AIME* **1969**, *245*, 1063–1074.
- Judd, R.R.; Paxton, H.W. Kinetics of Austenite Formation from a Spheroidized Ferrite-Carbide Aggregates. *Trans. TMS-AIME* **1968**, *242*, 206–215.
- Liu, Z.K.; Agren, J. Morphology of cementite decomposition in an Fe-Cr-C alloy. *Metall. Trans. A* **1991**, *22*, 1753–1759. [CrossRef]
- Liu, Z.K.; Hoglund, L.; Jonsson, B.; Agren, J. An experimental and theoretical study of cementite dissolution in an Fe-Cr-C alloy. *Metall. Trans. A* **1991**, *22*, 1745–1752. [CrossRef]

18. Goune, M.; Maugis, P.; Drillet, J. A Criterion for the Change from Fast to Slow Regime of Cementite Dissolution in Fe–C–Mn Steels. *J. Mater. Sci. Technol.* **2012**, *28*, 728–736. [[CrossRef](#)]
19. Taillard, R.; Verrier, P.; Maurickx, T. Retained Austenite in the C.G.H.A.Z. of 0.1 wt% C Si-alloyed Steels. *J. Phys. IV Colloq.* **1996**, *6*, 245–254. [[CrossRef](#)]
20. Borrajo-Pelaez, R.; Hedström, P. Recent Developments of Crystallographic Analysis Methods in the Scanning Electron Microscope for Applications in Metallurgy. *Crit. Rev. Solid State Mater. Sci.* **2018**, *43*, 455–474. [[CrossRef](#)]
21. Lolla, S.V.T. Understanding Microstructure Evolution in Rapid Thermal Processing of AISI 8620 Steel. Master's Thesis, The Ohio State University, Columbus, OH, USA, 2009.
22. Lolla, S.V.T.; Alexandrov, B.; Babu, S.; Cola, G. Towards Understanding the Microstructure Development during Heating and Cooling of Steels. Presented at the International Conference on Processing and Manufacturing of Advanced Materials-THERMEC'2009, Berlin, Germany, 25–29 August 2009.
23. Lolla, S.V.T.; Cola, G.; Narayanan, B.; Alexandrov, B.; Babu, S.S. Development of rapid heating and cooling (flash processing) process to produce advanced high strength steel microstructures. *Mater. Sci. Technol.* **2011**, *27*, 863–875. [[CrossRef](#)]
24. Cola, G. Properties of bainite nucleated by water quenching in 80 ms. In *1st International Symposium on Steel Science*; Furuhashi, T., Tsuzaki, K., Eds.; Iron and Steel Institute of Japan: Tokyo, Japan, 2007; pp. 187–190.
25. Papaefthymiou, S. A New Opportunity for the Design of Advanced High Strength Steels with Heterogeneous-Phase Microstructures via Rapid Thermal Processing. *J. Nanosci. Adv. Technol.* **2017**, *2*, 20–23. [[CrossRef](#)]
26. Cerda, F.M.C.; Goulas, C.; Sabirov, I.; Papaefthymiou, S.; Monsalve, A.; Petrov, R. Microstructure, texture and mechanical properties in a low carbon steel after ultrafast heating. *Mater. Sci. Eng. A* **2016**, *672*, 108–120. [[CrossRef](#)]
27. Knijf, D.D.; Puype, A.; Föjer, C.; Petrov, R. The influence of ultra-fast annealing prior to quenching and partitioning on the microstructure and mechanical properties. *Mater. Sci. Eng. A* **2015**, *627*, 182–190. [[CrossRef](#)]
28. Reis, A.C.; Bracke, L.; Petrov, R.; Kaluba, W.J.; Kestens, L. Grain refinement and texture change in interstitial free steels after severe rolling and ultra-short annealing. *ISIJ Int.* **2003**, *43*, 1260–1267. [[CrossRef](#)]
29. Lucas, A.; Paepe, A.D.; Petitgand, H.; Colin, C.; Chapuis, L.; Artimez, J. *Production of High-Quality Formable Grades in an Ultra Short Annealing Processing Line*; EU Publications: Luxemburg, 2007.
30. Puype, A. Developing of Advanced High Strength Steel via Ultrafast Annealing. Master's Thesis, Ghent University, Ghent, Belgium, 2014.
31. Li, X.; Ramazani, A.; Prahl, U.; Bleck, W. Quantification of complex-phase steel microstructure by using combined EBSD and EPMA measurements. *Mater. Charact.* **2018**, *142*, 179–186. [[CrossRef](#)]
32. Cerda, F.M.C.; Kestens, L.; Monsalve, A.; Petrov, R. The effect of ultrafast heating in cold-rolled low carbon steel: Recrystallization and texture evolution. *Metals* **2016**, *6*, 288. [[CrossRef](#)]
33. Cerda, F.M.C.; Kestens, L.; Petrov, R. “Flash” Annealing in a Cold-Rolled Low Carbon Steel Alloyed with Cr, Mn, Mo, and Nb: Part II—Anisothermal Recrystallization and Transformation Textures. *Steel Res. Int.* **2018**, *90*, 1–13.
34. Cerda, F.M.C.; Schulz, B.; Papaefthymiou, S.; Artigas, A.; Monsalve, A.; Petrov, R. The Effect of Ultrafast Heating on Cold-Rolled Low Carbon Steel: Formation and Decomposition of Austenite. *Metals* **2016**, *6*, 321. [[CrossRef](#)]
35. Cerda, F.M.C.; Sabirov, I.; Goulas, C.; Sietsma, J.; Monsalve, A.; Petrov, R. Austenite formation in 0.2% C and 0.45% C steels under conventional and ultrafast heating. *Mater. Des.* **2017**, *116*, 448–460. [[CrossRef](#)]
36. Cerda, F.M.C.; Vercruyse, F.; Goulas, C.; Schulz, B.; Petrov, R. ‘Flash’ Annealing in a Cold-Rolled Low Carbon Steel Alloyed With Cr, Mn, Mo, and Nb: Part I—Continuous Phase Transformations. *Steel Res. Int.* **2018**, *90*. [[CrossRef](#)]
37. Kaluba, W.; Taillard, R.; Foct, J. The bainitic mechanism of austenite formation during rapid heating. *Acta Mater.* **1998**, *46*, 5917–5927. [[CrossRef](#)]
38. Kaluba, W.; Taillard, R.; Foct, J. A reply to “discussion to “the bainitic mechanism of austenite formation during rapid heating””. *Scr. Mater.* **2000**, *42*, 511–516. [[CrossRef](#)]
39. Aaronson, H.; Nie, J. Discussion to “the bainitic mechanism of austenite formation during rapid heating”. *Scr. Mater.* **2000**, *42*, 505–509. [[CrossRef](#)]

40. Papaefthymiou, S.; Bouzouni, M.; Petrov, R. Study of carbide dissolution and austenite formation during ultra-fast heating in medium carbon chromium molybdenum steel. *Metals* **2018**, *8*, 646. [[CrossRef](#)]
41. Papaefthymiou, S.; Goulas, C.; Cerda, F.M.C.; Geerlofs, N.; Petrov, R. The Effect of Heating Rate on the Microstructure of a Soft-Annealed Medium Carbon Steel. *Steel Res. Int.* **2017**, *88*, 1700158. [[CrossRef](#)]
42. Bouzouni, M.; Papaefthymiou, S. Modeling of the Steel Microstructure Gained after the Application of an Ultra-Fast Heat Treatment. *J. Nanosci. Adv. Technol.* **2017**, *2*, 15–19. [[CrossRef](#)]
43. Bouzouni, M.; Papaefthymiou, S. Preliminary Study of Carbide Dissolution during an Ultra-Fast Heat Treatment in Chromium Molybdenum Steel. *Int. J. Metall. Met. Phys.* **2017**, *2*, 005.
44. Baniş, A.; Papaefthymiou, S. Microstructure Characterization of an Ultra-Fast Heated Medium Carbon Chromium-Manganese High Strength Steel. *Int. J. Metall. Met. Phys.* **2018**, *3*, 2631–5076.
45. Andersson, J.; Helander, T.; Höglund, L.; Shi, P.; Sundman, B. Thermo-Calc & DICTRA, computational tools for materials science. *Calphad* **2002**, *26*, 273–312.
46. Cayron, C. ARPGE: A computer program to automatically reconstruct the parent grains from electron backscatter diffraction data. *J. Appl. Crystallogr.* **2007**, *40*, 1183–1188. [[CrossRef](#)] [[PubMed](#)]
47. Kirkaldy, J.S.; Thomson, B.A.; Baganis, E.A. *Hardenability Concepts with Applications to Steel*; Kirkaldy, J.S., Doane, D.V., Eds.; AIME: Warrendale, PA, USA, 1978; p. 82.
48. Kirkaldy, J.S.; Venugopalan, D. *Phase Transformations in Ferrous Alloys*; Marder, A.R., Goldstein, J.I., Eds.; AIME: Warrendale, PA, USA, 1984; p. 125.
49. Bhadeshia, H.K.D.H. The Driving Force for Martensitic Transformation in Steels. *Met. Sci.* **1981**, *15*, 175–177. [[CrossRef](#)]
50. Bhadeshia, H.K.D.H. A Thermodynamic Analysis of Isothermal Transformation Diagrams. *Met. Sci.* **1982**, *16*, 159–165. [[CrossRef](#)]
51. Lee, S.J.; Lee, Y.K. Effect of austenite grain size on martensitic transformation of a low alloy steel. *Mater. Sci. Forum* **2005**, *475–479*, 3169–3172. [[CrossRef](#)]
52. Petrov, R.; Kestens, L.; Wasilkowska, A.; Houbaert, Y. Microstructure and texture of a lightly deformed TRIP-assisted steel characterized by means of the EBSD technique. *Mater. Sci. Eng. A* **2007**, *447*, 285–297. [[CrossRef](#)]
53. Pinard, P.; Schwedt, A.; Ramazani, A.; Prahl, U.; Richter, S. Characterization of dual-phase steel microstructure by combined submicrometer EBSD and EPMA carbon measurements. *Microsc. Microanal.* **2013**, *19*, 996–1006. [[CrossRef](#)] [[PubMed](#)]
54. Szabo, P.J.; Szalai, I. Effect of Monotonic and Cyclic Deformation on the IQ-Maps of Austenitic Stainless Steel. *Mater. Sci. Forum* **2005**, *473–474*, 267–272. [[CrossRef](#)]
55. Wu, J.; Wray, P.J.; Garcia, C.I.; Hua, M.; Deardo, A.J. Image quality analysis: A new method of characterizing microstructures. *ISIJ Int.* **2005**, *45*, 254–262. [[CrossRef](#)]
56. Cerda, F.M.C.; Schulz, B.; Celentano, D.; Monsalve, A.; Sabirov, I.; Petrov, R. Exploring the microstructure and tensile properties of cold-rolled low and medium carbon steels after ultrafast heating and quenching. *Mater. Sci. Eng. A* **2019**, *745*, 509–516. [[CrossRef](#)]

